JGR Space Physics

RESEARCH ARTICLE
10.1029/2023JA031621

Waves in Magnetosheath Jets—Classification and the Search for Generation Mechanisms Using MMS Burst Mode Data

E. Krämer[1], M. Hamrin[1], H. Gunell[1], T. Karlsson[2], K. Steinvall[3], O. Goncharov[4], and Mats André[3]

[1]Departement of Physics, Umeå University, Umeå, Sweden, [2]Division of Space and Plasma Physics, School of Electrical Engineering and Computer Science, KTH Royal Institute of Technology, Stockholm, Sweden, [3]Swedish Institute of Space Physics, Uppsala, Sweden, [4]Faculty of Mathematics and Physics, Charles University, Prague, Czech Republic

Key Points:

- MMS burst mode data is used to investigate waves in, and in the vicinity of, magnetosheath jets
- 0.2 Hz waves, 1 Hz waves, whistler waves, electron acoustic waves, lower hybrid waves, and solitary waves are observed
- Waves with low frequencies cannot be explained by "basic" wave modes that are derived in homogeneous plasmas

Supporting Information:

Supporting Information may be found in the online version of this article.

Correspondence to:

E. Krämer,
eva.kramer@umu.se

Citation:

Krämer, E., Hamrin, M., Gunell, H., Karlsson, T., Steinvall, K., Goncharov, O., & André, M. (2023). Waves in magnetosheath jets—Classification and the search for generation mechanisms using MMS burst mode data. *Journal of Geophysical Research: Space Physics*, *128*, e2023JA031621. https://doi.org/10.1029/2023JA031621

Received 20 APR 2023
Accepted 22 JUN 2023

Abstract Magnetosheath jets are localized dynamic pressure enhancements in the magnetosheath. We make use of the high time resolution burst mode data of the Magnetospheric Multiscale mission for an analysis of waves in plasmas associated with three magnetosheath jets. We find both electromagnetic and electrostatic waves over the frequency range from 0 to 4 kHz that can be probed by the instruments on board the MMS spacecraft. At high frequencies we find electrostatic solitary waves, electron acoustic waves, and whistler waves. Electron acoustic waves and whistler waves show the typical properties expected from theory assuming approximations of a homogeneous plasma and linearity. In addition, 0.2 Hz waves in the magnetic field, 1 Hz electromagnetic waves, and lower hybrid waves are observed. For these waves the approximation of a homogeneous plasma does not hold anymore and the observed waves show properties from several different basic wave modes. In addition, we investigate how the various types of waves are generated. We show evidence that, the 1 Hz waves are connected to gradients in the density and magnetic field. The whistler waves are generated by a butterfly-shaped pitch-angle distribution and the electron acoustic waves by a cold electron population. The lower hybrid waves are probably generated by currents at the boundary of the jets. As for the other waves we can only speculate about the generation mechanism due to limitations of the instruments. Studying waves in jets will help to address the microphysics in jets which can help to understand the evolution of jets better.

Plain Language Summary There is a constant plasma flow from the sun, the solar wind. The Earth's magnetic field deflects the solar wind as it flows toward Earth. As the solar wind plasma approaches Earth it gets decelerated and heated at the bow shock. Earthward of the bow shock, the magnetosheath is located where the flow diverges around Earth. In the magnetosheath plasma flows that are denser and faster than normal can sometimes be observed, so called magnetosheath jets. We investigate waves in plasmas in these magnetosheath jets and how they are generated. Studying these waves will help to understand the interaction of magnetosheath jets with their environment.

1. Introduction

Magnetosheath jets are dynamic pressure enhancements resulting from a either velocity increase, a density increase, or a combination of both (Archer & Horbury, 2013). There has been a great interest in magnetosheath jets in recent years (see Plaschke et al. (2018) for an overview), but the evolution and the formation mechanisms of jets are still under debate. While the boundaries of jets are marked by density or velocity increases, the magnetic field inside jets often decreases or increases in comparison with the surrounding magnetosheath plasma (Plaschke et al., 2013). This causes magnetic field and density gradients in the vicinity of the jet. These gradients potentially generate a variety of waves as the plasma inside and outside the jets has different properties. Raptis et al. (2022) showed that the particle distributions inside jets are highly variable and there can be two plasma populations present. Waves can transfer energy between particle distributions through wave-particle interactions. Therefore, it is of interest to study waves inside, and in the vicinity of, jets.

Previous studies have revealed some typical properties of jets (Plaschke et al. (2018) and references therein). Magnetosheath jets have a typical size of about 0.1 Earth radii (R_E) (Plaschke et al., 2020) but the morphology of jets is still under debate (Plaschke et al., 2018). Note, in the literature there are also other names used for these

dynamic pressure enhancements (Plaschke et al., 2018). For example, Gunell et al. (2014) called them plasmoids and Plaschke et al. (2013) called them high-speed jets.

The occurrence rate of jets depends on the angle θ_{Bn} between the interplanetary magnetic field $\vec{B}_{IMF}$ (IMF) and the bow shock normal $\vec{n}$ (Plaschke et al., 2013). The bow shock and the magnetosheath are considered to be quasi-parallel if $\theta_{Bn} < 45°$ and quasi-perpendicular if $\theta_{Bn} > 45°$. The formation mechanisms of magnetosheath jets are still under debate but they are often associated with phenomena at the quasi-parallel bow shock and therefore the foreshock (Plaschke et al., 2018). The foreshock is the region upstream of the quasi-parallel bow shock, penetrated by reflected particles from the bow shock (Eastwood et al., 2005).

The magnetosheath itself is a highly turbulent region where a variety of waves in plasma can be observed. Commonly observed electromagnetic waves are mirror mode waves, Alfvén/ion-cyclotron waves and whistler waves (Lucek et al., 2005). An ion temperature anistropy where $T_{i\perp} > T_{i\parallel}$ can excite either the ion-cyclotron instability or the mirror mode instability depending on plasma-β (Gary, 1992). Taking into account a small Helium population, Gary et al. (1993) showed that for $\beta < 1$ the proton-cyclotron modes dominates while for $\beta > 2$ the mirror mode is excited. Whistler waves in the magnetosheath are often observed in local magnetic minima (Smith & Tsurutani, 1976) and their generation has been associated with the local temperature anisotropy (Huang et al., 2018; Kennel & Petschek, 1966). Lower hybrid waves have been reported close to the magnetopause associated with magnetopause reconnection (Pritchett et al., 2012). These lower hybrid waves are suggested to be generated by strong density gradients (Krall & Liewer, 1971; Pritchett et al., 2012). In addition, different kinds of electrostatic waves have been reported (Rodriguez, 1979). The authors report a high frequency component close to the electron plasma frequency f_{pe}, a low frequency component at the ion plasma frequency f_{pi}, and a intermediate component $f_{pi} < f < f_{pe}$. Pickett et al. (2005) suggested that electrostatic solitary structures could be generated by counter-streaming electrons.

Raptis et al. (2022) reported a jet which exhibits a strongly variable ion velocity distribution consisting of two ion populations. The authors suggest that the variations in the ion velocity distribution is the result of the jet interacting with the magnetosheath plasma. Such a plasma could drive a variety of different waves. So far, there have been only two attempts to investigate waves in magnetosheath jets systematically namely by Gunell et al. (2014) and Karlsson et al. (2018). In addition, a study by Blanco-Cano et al. (2020) investigated the magnetosheath microstructure, which included a short discussion of wave activity inside and outside jets. None of these previous studies have investigated the sources of these waves with respect to local plasma parameters using spacecraft data. Locally generated waves can transfer energy between particle distributions and can therefore change properties of jets. Consequently, it is of interest to study waves and their sources in, and in the vicinity of, magnetosheath jets.

The first study on waves in jets by Gunell et al. (2014) used data from the Cluster mission. They reported an increase in wave activity inside jets (plasmoids in their terminology). They observed both whistler waves and waves in the lower hybrid frequency range. The authors noted that an increased speed of the jet in comparison to the surrounding plasma provides energy for the generation of waves which has also been reported in laboratory experiments (Hurtig et al., 2005). In these experiments currents are seen to develop at boundaries of laboratory jets. Such currents drive lower hybrid waves. Gunell et al. (2014) suggested that whistler waves are driven by beams that form from the acceleration of electrons. These electrons are accelerated by electric fields parallel to the magnetic field which are formed by the interaction of the jet with the magnetosheath plasma. However, the sources of the waves were not further investigated using data. The study did not find any waves with frequencies higher than the whistler mode waves, most likely due to the low time resolution of the data.

The second study on waves in jets by Karlsson et al. (2018) used survey and fast mode data from the magnetospheric multiscale (MMS) mission. The authors also reported whistler waves and wave activity in the lower hybrid frequency range in agreement with Gunell et al. (2014). In addition, they reported broadband electrostatic waves extending above the electron gyrofrequency as well as quasi-periodic low frequency electromagnetic waves with a period of about 10 s. The authors suggested that the broadband electrostatic waves are related to broadband electrostatic noise (BEN) which could be associated with ion acoustic or Langmuir waves. According to them, the BEN is the signature of solitary waves in a spectrum. The low frequency electromagnetic waves have a large compressional component and where only observed in jets that are located in the quasi-parallel magnetosheath. It was suggested that these waves are associated with ultra-low frequency (ULF) waves that form in the foreshock and convect into the magnetosheath. The authors did not investigate the sources of the waves in the

lower hybrid frequency range or the whistler waves further. Karlsson et al. (2018) also investigated the energy of jets dissipated through waves and found that only the low frequency waves are possibly energetically important.

Another study by Blanco-Cano et al. (2020) examined the magnetosheath microstructure. They also investigated low frequency waves both inside and outside of jets using MMS data. They reported mirror mode waves outside of jets and waves with larger transverse components inside of jets. The authors suggested that the wave inside of jets could be a combination of several different wave modes, but they did not investigate it further.

In this paper, for the first time, we make use of high resolution data to investigate waves observed in jets. We report and discuss the different observed waves, give their properties and discuss their sources. We also discuss the limitations of approximations that are commonly used to derive wave properties. This is a step toward understanding the microphysics in jets which can help to understand the formation and evolution of jets better. This paper is structured as follows. First, the data and the methods that are used will be described in Section 2. Then, in Section 3, a detailed analysis of waves in one magnetosheath jet will be presented which includes a discussion of the wave generation. Furthermore, two more magnetosheath jets are briefly discussed in Section 4. Finally, in Section 5, we discuss similarities and differences between the jets.

2. Instrumentation and Methods

Data from the Magnetospheric Multiscale (MMS) mission (Burch et al., 2016) are used in this work. We use data from the Fluxgate Magnetometer (FGM) (Russell et al., 2016) for the magnetic field vector. The data used have 128 samples per second in burst mode and 16 samples per second in fast mode. For variations in the magnetic field, the AC magnetic field vector is obtained from the search coil magnetometer (SCM) (Le Contel et al., 2016). In burst mode the data are provided with 8192 samples per second and in survey mode with 32 samples per second. In SCM burst mode data can be used to study magnetic field variations in 1–4,096 Hz. The Electric field Double Probe (EDP) (Ergun et al., 2016; Lindqvist et al., 2016) provides measurements of the electric field vector. The burst mode data have 8192 samples per second and 32 samples per second in fast mode. Finally, we use the Fast Plasma Investigation (FPI) (Pollock et al., 2016) instrument for the ion and electron distributions as well as moments derived from them. The burst mode data have a time resolution of 30 ms for the electron data and 150 ms for the ion data.

For the IMF and solar wind properties propagated to the bow shock nose, the OMNI data set is used (Papitashvili & King, 2020).

All data are presented in Geocentric Solar Ecliptic coordinates if not otherwise stated. If single spacecraft measurements are shown, data from the MMS1 spacecraft are used. We also make use of a field aligned coordinate (FAC) system with respect to a background magnetic field $\vec{B}$. The FAC system is constructed so that the parallel component is $\hat{e}_{\parallel} \parallel \vec{B}$, the perpendicular components are $\hat{e}_{\perp 1} \parallel \left(\hat{e}_{\parallel} \times \vec{x}_{GSE}\right)$, and $\hat{e}_{\perp 2} \parallel (\hat{e}_{\parallel} \times \hat{e}_{\perp 1})$.

Whenever a background magnetic field $\vec{B}$ is used, it refers to the magnetic field measured by the FGM instrument. The AC magnetic field $\delta\vec{B}$ is chosen depending on the frequency range that is investigated. For wave activity above 1 Hz data from the SCM instrument are used. For wave activity close to and below 1 Hz a filter frequency f_{filt} is chosen. Then the FGM data are low pass filtered with a cut-off frequency f_{filt} to get an estimate for the background magnetic field $\vec{B}$. The FGM data are also high pass filtered to get an estimate of the AC magnetic field $\delta\vec{B}$. Note, if the high passed filtered FGM data are used for wave activity, only waves with frequencies up to 64 Hz can be investigated due to the limitations of the sampling frequency of 128 Hz (in burst mode).

The bow shock normal $\vec{n}$ is estimated using a three-dimensional model for the bow shock by Formisano (1979). We determined $\vec{n}$ at the minimum distance to the bow shock along the plasma flow direction in the magnetosheath. The upstream data were averaged over 4 min before and after the observation of a jet. The flow direction was calculated using the median value of measurements 5 min before and after the observation of a jet.

The current density $\vec{j}$ is estimated using the curlometer method using data from the FGM (Dunlop et al., 1988). The method makes use of magnetic field measurements from all four spacecraft to estimate the current density according to Ampere's law.

In the literature, different methods have been used to identify magnetosheath jets (see Table 1 in Plaschke et al. (2018) for an overview). These methods can be categorized whether the dynamic pressure $P_d = mn_i v_i^2$ is compared to upstream conditions or averaged local conditions (Plaschke et al., 2018). A commonly used criteria, using upstream conditions, is the Plaschke et al. (2013) criteria, but his method can only be used in the in the subsolar regime ($\theta_s < 30°$ where $\theta_s = \arccos(x_{GSE}/r)$ with r the distance to the Earth's center). Since we do not want to constrain our study to jets in the subsolar region, we use averaged local conditions for the imposed threshold. In this study the method of Archer and Horbury (2013) is used. Magnetosheath plasma is identified as a jet if it exceeds the threshold of two times the background dynamic pressure $P_d > 2\langle P_d \rangle$. The background dynamic pressure $\langle P_d \rangle$ is calculated from an running average over 20 min using local magnetosheath conditions.

In this study we investigate three jets in total. The jets are chosen from the data set described in Goncharov et al. (2020). The data set was reduced to jet events where burst mode data are available. Based on the remaining subset we chose three jets in different magnetosheath regions under different magnetosheath conditions.

3. Observations

In the following, a magnetosheath jet which was observed on 3 January 2018, between 19:41:49.9–59.3 UT, is presented and analyzed in more detail. The jet was observed by the MMS spacecraft which were located at $\vec{r}_{\mathrm{GSE}} \approx (9.4, 7.1, 3.9)\,\mathrm{R_E}$, corresponding to a solar zenith angle $\theta_s = 41°$. The angle between the IMF and the bow shock normal is $\theta_{\mathrm{Bn}} \approx 46°$ which indicates that the jet is located in the quasi-perpendicular magnetosheath. During this jet observation the configuration of the four MMS spacecraft was a potato-shaped tetrahedron with an elongation of 0.45 and a planarity of 0.57 according to the classification by Robert et al. (1998). For a regular tetrahedral configuration all interspacecraft distances would be the same which corresponds to a planarity of 0. The potato-shaped spacecraft configuration is therefore not optimal for four-spacecraft-analysis.

Figure 1 gives an overview over the observations. Figure 1A shows the MMS1 data (Figures 1Aa–A1e) and the upstream magnetic field propagated to the bow shock (Figure 1Af) over a 20 min interval centered around the jet. We present the magnetic field $\vec{B}$, ion energy spectrum E_i, ion velocity $\vec{v}_i$, ion and electron densities n_i, n_e, and dynamic pressure P_d of the surrounding magnetosheath. The black, vertical lines highlight the time where burst mode data is available between 19:41:33–42:23 UT. Figure 1Ae shows the dynamic pressure P_d as well as the threshold of twice the average dynamic pressure $2\langle P_d \rangle$, which is calculated over a 20 min running average. The dynamic pressure exceeds the threshold three times during a time interval of 75 s between 19:40:45–42:00 UT. Previous studies (e.g., Raptis et al., 2020) have considered such data to correspond to one jet instead of three separate jets. In the following we will only investigate the last and also highest peak in dynamic pressure since data in burst mode is only available during this time.

An overview over the burst mode data is presented in Figure 1B. These data will be described in detail in the following paragraphs. The black, vertical lines in Figure 1B mark the time where the jet is observed as the dynamic pressure P_d exceeds the threshold $2\langle P_d \rangle$ (Figure 1Bh). In addition, the spatial configuration of the four MMS spacecraft is shown in Figure 1C. The distance between the spacecraft varies between 17 km (MMS1 and MMS4) and 40 km (MMS3 and MMS4).

The magnetic field direction is the same before and after the jet but inside the jet there is a rotation of the magnetic field $\vec{B}$ (Figure 1Bc). This rotation leads to an increase in the current density (Figure 1Bi). Figure 1Bf shows the density from all four spacecraft which indicate that there are density gradients present. For example, Figure 1Bg shows the magnetic field magnitude from all four spacecraft which also indicates that there are magnetic field gradients present. Therefore the plasma environment cannot be considered homogeneous at the edges of the jet.

The AC magnetic field $\delta\vec{B}$ (Figure 1Bb) shows an increased wave activity at different frequencies inside, and in the vicinity of, the jet between 19:41:48–42:03. We compute the AC magnetic field spectrum $P(B)$ of the magnetic field magnitude using a continuous wavelet transform (Figure 1Bj), and use the same method to calculate the electric field spectrum $P(E)$ of the electric field magnitude (Figure 1Bk). The electric field $\vec{E}$ (Figure 1Bc) also shows an increase in wave activity inside the jet between 19:41:50–58 UT.

To further investigate these waves, we make use of the methods for wave propagation analysis developed by Santolík et al. (2003). It can be used to obtain estimates for the angle θ_k which is the angle between the wave vector and the background magnetic field (Figure 1Bl). The method also gives an estimate for the ellipticity ϵ of

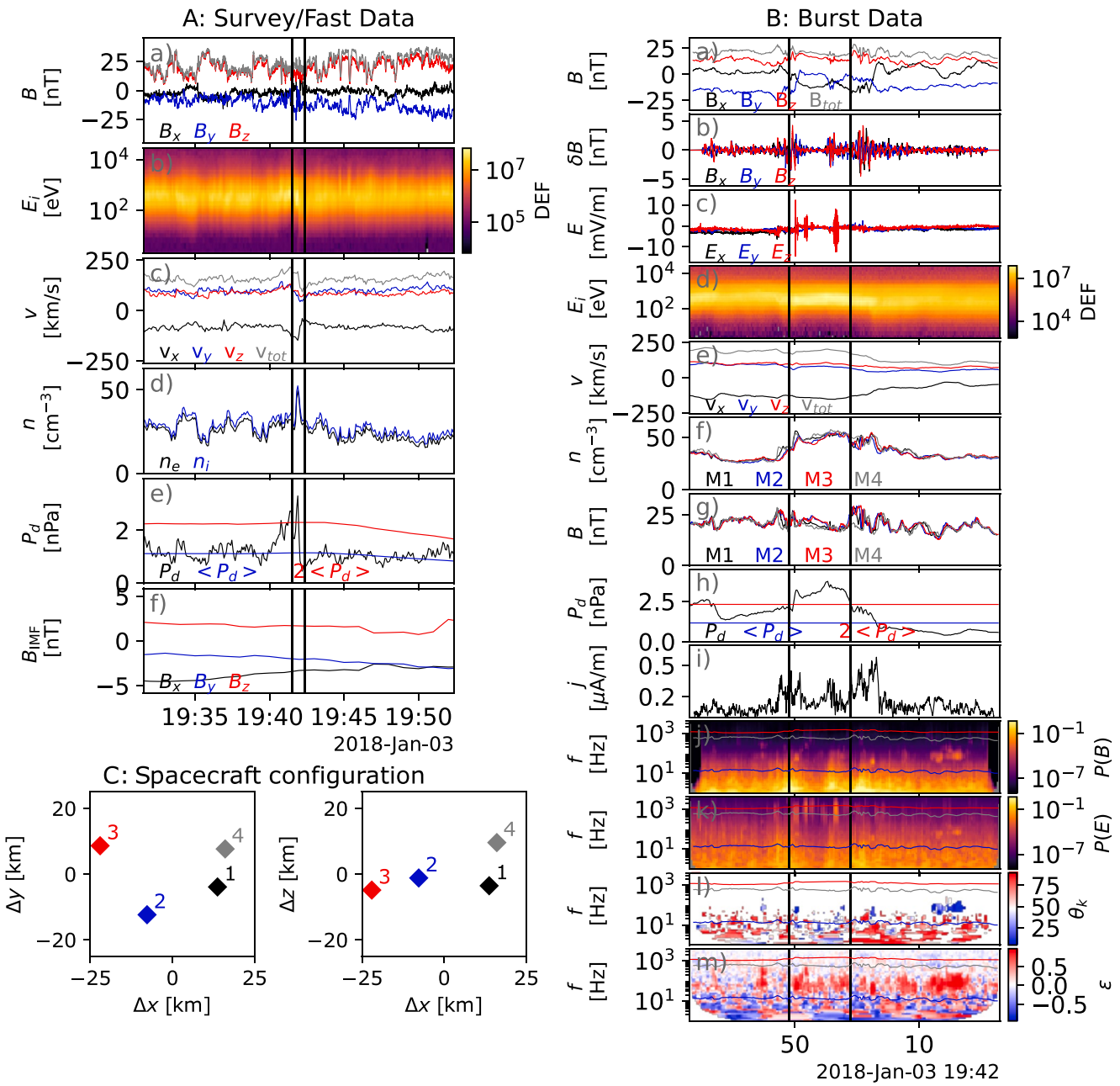

Figure 1. Overview over the event. A: 20 min overview of surrounding magnetosheath: (a) magnetic field $\vec{B}$, (b) ion energy spectrum E_i in units of [keV/(cm^2 s sr keV)], (c) ion velocity $\vec{v}_i$, (d) ion and electron densities n_i, n_e, (e) dynamic pressure P_d, including averaged dynamic pressure $\langle P_d \rangle$, and (f) interplanetary magnetic field $\vec{B}_{IMF}$. The vertical black lines indicate the time interval where burst mode data is available. B: overview over burst mode data. (a) Magenetic field $\vec{B}$, (b) AC magnetic field $\delta\vec{B}$, (c) electric field $\vec{E}$, (d) ion energy spectrum E_i in units of [keV/(cm^2 s sr keV)], (e) ion velocity $\vec{v}_i$, (f) ion density n_i from MMS1-4, (g) magnetic field magnitude $|B|$ from MMS1-4, (h) dynamic pressure P_d including averaged magnetic pressure $\langle P_d \rangle$ and the threshold $2\langle P_d \rangle$, (i) current density $|\vec{j}|$, (j) magnetic field spectrum $P(B)$ in units of [(nT)^2/Hz], (k) electric field spectrum $P(E)$ in units of [(mV/m)^2/Hz], (l) propagation angle θ_k with respect to the magnetic field, and (m) ellipticity ϵ. The colored curves in the spectra (j–m) indicate the following natural frequencies: the lower hybrid frequency $f_{\rm lh}$ in blue, the electron cyclotron frequency $f_{\rm ce}$ in gray, and the ion plasma frequency $f_{\rm pi}$ in red. The vertical black lines indicate the jet. C: The MMS spacecraft configuration in the *xy*-plane (left) and the *xz*-plane (right).

the AC magnetic field. The ellipticity ϵ is defined as the ratio of the two axes of the polarization ellipse $\epsilon = a/b$ where $a \leq b$ such that $|\epsilon| \leq 1$. An ellipticity $\epsilon = +1$ corresponds to a right-handed circularly polarized wave, $\epsilon = 0$ corresponds to a linear polarized wave, and $\epsilon = -1$ corresponds to a left-handed circularly polarized wave. The ellipticity ϵ is shown in Figure 1Bm, showing that waves of different polarization are present.

We will investigate the following types of waves that show an increased activity inside the jet: electromagnetic waves with a frequency of approximately 1 Hz that have an increased amplitude close to edge of the jet (Figures 1Bb and 1Bc); higher frequency electromagnetic waves (increased wave activity around 100 Hz in Figures 1Bj and 1Bk); electrostatic waves as well as electrostatic solitary waves, both are seen in Figure 1Bc and as wave activity above 100 Hz in 1Bk; electromagnetic wave activity in the range of $5 - 200$ Hz. In particular, we are going to compare the observed waves with wave modes and their properties as they are derived in their simplest form (e.g., as they are derived in textbooks). We will refer to these wave modes as "basic" wave modes. We will then also discuss whether these approximations hold or a more complex picture needs to be taken into account. In addition, we will discuss possible generation mechanisms. We consider waves to be electrostatic if we only observe a signal in the electric field data but not in the magnetic field data.

The data used are available with 8192 samples per second, thus we will only investigate waves with frequencies smaller than 4 kHz. This excludes for example, electron plasma waves since the plasma frequency of electrons is approximately 6 kHz.

We will first describe the properties of each wave. Then the wave mode will be identified, if possible, and the source of each wave will be investigated.

3.1. 1 Hz Electromagnetic Waves

Close to the edge of the magnetosheath jet, around 19:41:50 UT and 19:42:00 UT, there is an increased wave activity in the magnetic field with frequencies around 1 Hz (Figures 1Bb and 1Bj). To examine these waves further, also below 1 Hz, the background magnetic field $\vec{B}$ and the AC magnetic field $\delta\vec{B}$ are constructed using a low-pass filter frequency of 0.33 Hz as described in Section 2. This frequency was chosen to examine waves that have at least three periods within the jet which has a duration of 10 s. Using a lower frequency would be equivalent to considering the jet itself as a wave. Figure 2 gives an overview over these waves and their properties.

The calculated background magnetic field $\vec{B}$ is shown in Figure 2a, the AC magnetic field $\delta\vec{B}$ in FAC is shown in Figure 2b and its spectrum in Figure 2c. The electric field spectrum is shown in Figure 2d and the ion density n_i in Figure 2e. To examine variations in the ion density δn_i (Figure 2f) and ion velocity components $\delta\vec{v}_i$ (Figure 2g), the same filter frequency is used as for $\delta\vec{B}$. In addition, the threshold for the mirror mode wave $C_m = 1 + \beta_\perp(1 - T_\perp/T_\parallel) < 0$ is given (Kivelson & Russell, 1995) (Figure 2h). The magnetic pressure $P_{\mathrm{mag}} = B^2/2\mu_0$, thermal pressure $P_{\mathrm{th}} = nk_BT$ (Figure 2i) and the dynamic pressure P_d including the threshold $2\langle P_d\rangle$ (Figure 2j) are given. The vertical lines highlight the two wave packets with increased wave amplitudes (Figures 2b and 2c).

$\delta\vec{B}$ reaches amplitudes of up to 6 nT (Figure 2b at 19:42:01 UT) and the increased wave activity is observed for about 4 s, both at the leading edge of the jet around 19:41:48 UT and the trailing edge of the jet around 19:42:01 UT. The waves are observed when there is an increase or a decrease in n_i (Figure 2e). Figure 2f shows that $\delta B_\parallel$ is anti-correlated with δn_i. This anti-correlation is most prominent around 19:41:50 UT and 19:42:00 UT. $\delta B_\perp$ and $\delta B_\parallel$ have similar amplitudes (Figure 2b). Figure 2g shows $\delta\vec{v}_i$ which has also an increased amplitude during times of increased wave activity. Figure 2i shows that P_{th} and P_{mag} are anti-correlated (e.g., around 19:42:00 UT).

The phase velocity of waves can be determined using wave packets from all four MMS spacecraft and time-shift these wave packets so that their wave forms overlap. In order to estimate the phase speed of the 1 Hz electromagnetic waves we used δn_i from all four MMS spacecraft. Since this was only done to get a rough estimate of the speed, we used a simple eye inspection to determine the best overlap. For the first wave packet this results in a speed of 60 km s^{-1} and for the second packet in a speed of 90 km s^{-1} in the spacecraft frame. This corresponds to a propagation speed of about 160 km s^{-1} and 140 km s^{-1} in the plasma reference frame. Note, the potato–shaped tetrahedral spacecraft configuration is not optimal and the velocity is just an estimate.

To our knowledge, there is no basic wave mode that explains all the properties of the above described wave. Nevertheless, there are several wave modes that can explain some of the properties, namely slow mode waves, mirror mode waves, and electromagnetic ion cyclotron waves. The typical properties of these waves will be discussed in the following.

The anti-correlation of $\delta B_\parallel$ and δn_i suggests the mirror mode as a possible wave mode (Figure 2f). This is also supported by the anti-correlation of P_{th} and P_{mag} (Figure 2i). Basic mirror modes, as they are derived using magnetohydrodynamic approximations, are non-propagating waves in the plasma reference frame (Southwood &

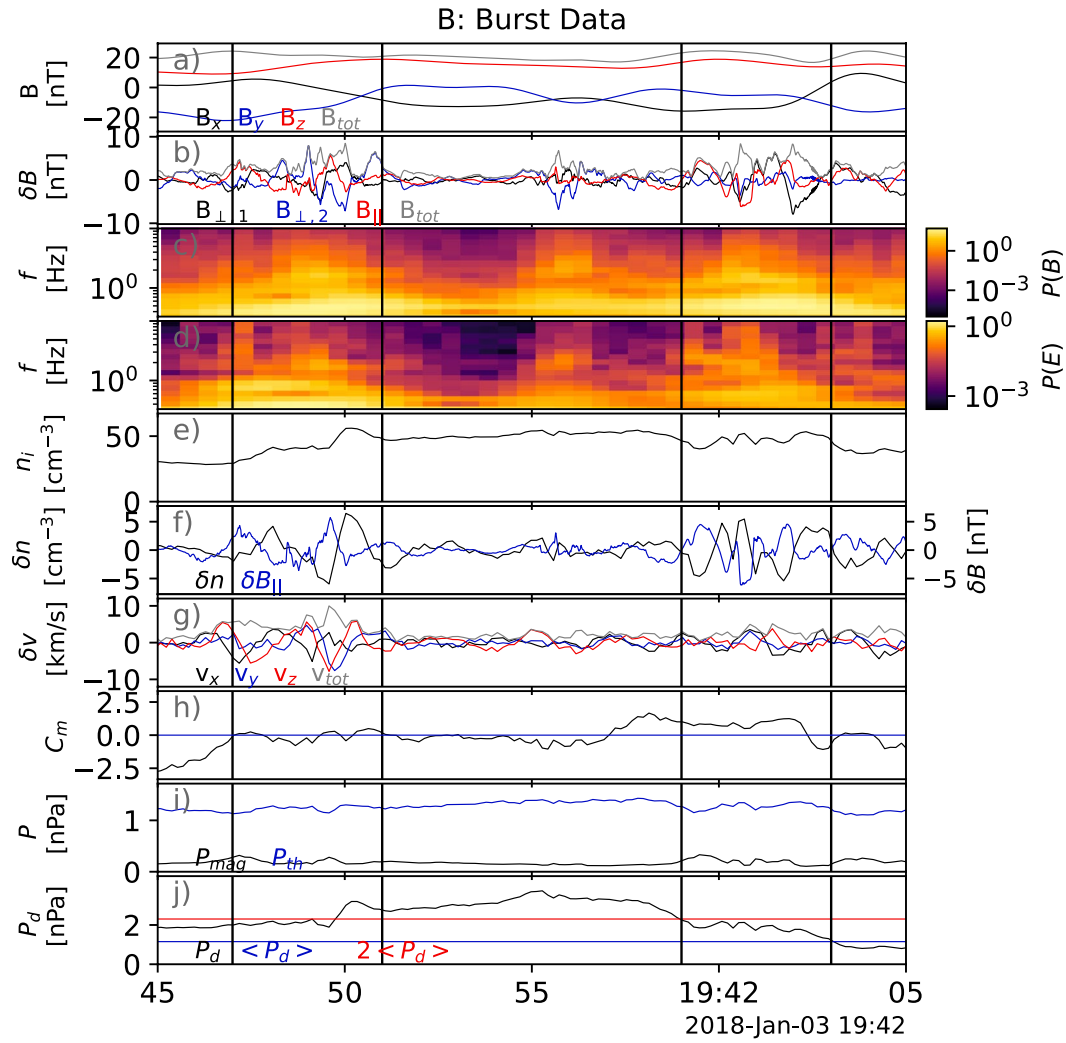

Figure 2. 1 Hz electromagnetic waves. (a) Background magnetic field $\vec{B}$, (b) AC magnetic field $\delta\vec{B}$, (c) magnetic field spectrum $P(B)$ in units of [(nT)^2/Hz], (d) electric field spectrum $P(E)$ in units of [(mV/m)^2/Hz], (e) ion density n_i, (f) variation in the ion density n_i and the in parallel magnetic field $\delta B_{||}$, (g) variations in the ion velocity $\delta\vec{v}_i$, (h) instability threshold for mirror mode C_m, (i) magnetic pressure P_{mag}, thermal pressure P_{th}, (j) dynamic pressure P_d and background dynamic pressure $\langle P_d \rangle$. The vertical black lines indicate the two wave packets discussed in the text.

Kivelson, 1993). The instability threshold for mirror modes is shown in Figure 2h where $C_m < 0$ for the plasma to support mirror mode waves. For the packet around 19:42:00 UT the plasma does not supports mirror mode waves as $C_m > 0$ and these waves should be heavily damped. However, for the packet around 14:41:50 UT, the plasma might support mirror mode waves as $C_m \approx 0$. For the smaller packet observed around 19:41:56 UT $C_m < 0$ such that the plasma can support mirror modes. Note, gradients in the magnetic field and density can modify mirror modes to non-zero real frequency waves, implying that they can be propagating in the plasma reference frame (Hasegawa, 1969), so called drift mirror modes. In addition, finite ion-Larmor radius effects cause a decrease in the stability threshold (Pokhotelov et al., 2004). This effect is likely to be relevant as the wavelength of the wave is of the order of 100 km and the ion-Larmor radius is of the order of 60 km. Therefore, we expect the resulting mirror mode threshold to be lower than indicated by C_m. The observed waves are propagating and exist when $C_m > 0$, which suggests that these waves are not locally generated mirror modes.

Slow mode waves also show anti-correlated $\delta B_{||}$ and δn_i, as well as an anti-correlation of $P_{\rm th}$ and $P_{\rm mag}$. In comparison to mirror modes, slow modes waves are propagating with velocities smaller than the Alfvén speed $v_A \approx$ 50–100 km s^{-1} in the plasma reference frame. We determined the velocity of the observed waves to be

138 km s^{-1} and 160 km s^{-1}. Thus, the observed waves propagate with speeds higher than the local Alfvén speed which suggests that the waves are not basic slow mode waves.

Slow mode waves or mirror mode waves could only account for $\delta B_{\parallel}$ and δn_i, but not for $\delta B_{\perp}$ which has a comparable amplitude to $\delta B_{\parallel}$.

Electromagnetic ion cyclotron (EMIC) waves exhibit variations in the perpendicular magnetic field and should be observed below the ion cyclotron frequency f_{ci} which is around $0.3 - 0.4$ Hz for protons. EMIC waves are predicted to propagate quasi-parallel to the background magnetic field. Due to their nonzero propagation velocity they should be Doppler shifted in the spacecraft frame. As described previously, we found that the wave propagates below the plasma flow speed. We interpret this result as the wave is moving away from the spacecraft which results in an observed frequency that is similar or lower than the frequency in the non-moving plasma frame. This indicates that EMIC waves would be observed at frequencies lower than f_{ci}. Therefore, an electromagnetic ion cyclotron wave, as they are derived for a homogeneous plasma, cannot explain our observations.

The dispersion relation and other typical properties for the previously discussed wave modes are usually derived in the context of a homogeneous plasma, which cannot be assumed here since the waves are observed when there is a change in density and rotation in the magnetic field. For example, we estimated the density to approximately increase with up to 40% within one wavelength for the first packet. Furthermore, for linear theory the variations are assumed to be much smaller than the background magnetic field. This cannot necessarily be assumed for waves with an amplitude of 6 nT compared to the ambient magnetic field with about 20 nT. Therefore, it might not be possible to reduce the observed waves to one of the basic wave modes. An additional complication is the fact that the waves could have been generated elsewhere and propagated to the position of the spacecraft. The fact that the 1 Hz waves are associated with the density gradient and magnetic field rotation it points to a local generation of the wave instead of a propagation from elsewhere.

Omidi and Winske (1995) simulated propagating mirror mode waves which could not be linked to a basic wave mode. The authors call them Mirror and Slow (MEOW) waves as they have properties between slow mode waves and mirror mode waves. Another possibility is that the 1 Hz waves might be a superposition of several different modes. Similarly, Sahraoui et al. (2003) reported the superposition of the slow mode, mirror mode and Alfvén mode in the magnetosheath using the k-filtering technique. Zhao et al. (2019) suggested the simultaneous existence of electromagnetic ion cyclotron waves and mirror modes in the magnetosheath.

The 1 Hz electromagnetic waves cannot be described by the properties of a basic wave mode but exhibits properties of several different wave modes instead. We suggest that the commonly used approximations, such as homogeneity, fail to describe this wave mode due to the non-homogeneous plasma environment.

3.2. Whistler Waves

In Figures 1Bj and 1Bk there are several occurrences where there is an increase of wave activity in the magnetic and electric spectrum in the frequency range 50–200 Hz. The polarization analysis shows an ellicpicity $\epsilon \approx 1$ (red in Figure 1Bm) and a propagation angle $\theta_k \approx 0$ (blue in Figure 1Bl) for these wave occurrences. We will now show and discuss one of these wave occurrences which was observed between 19:41:50.2–50.7 UT in more detail.

An overview of the observation is given in Figure 3, where Figure 3A gives a broader overview over the surrounding plasma between 19:41:48–52 UT and Figure 3B shows the packet between 19:41:50.1–50.8 UT.

The wave is observed with a frequency $f \approx$ 50–100 Hz (Figures 3Ac and 3Bb) which is approximately $0.1 f_{\mathrm{ce}}$ with f_{ce} as the electron cyclotron frequency. As seen in Figure 3Ba, the oscillations are mainly in the perpendicular magnetic field $\delta B_{\perp}$, corresponding to a small $\theta_k < 25°$ (Figure 3Be). Similar wave activity can also be observed in the electric field $\vec{E}$ (Figure 3Bb). The amplitude of these waves is about 0.4 nT and the duration of the observed packet is about 0.5 s. The propagation angle is small with respect to $\vec{B}$ (Figure 3Be). The ellipticity $\epsilon \approx +1$ (Figure 3Bf), corresponding to a right handed, circularly polarized wave. The wave is observed during a local minimum of the total magnetic field (Figure 3Aa) and there is an electron temperature anisotropy with $T_{e\parallel} > T_{e\perp}$ (Figure 3Ah). During the wave activity, we observed a butterfly-shaped electron pitch-angle distribution (Figure 3Ai).Similar wave activity can be seen throughout the jet, but also outside of the jet as seen in Figure 1B.

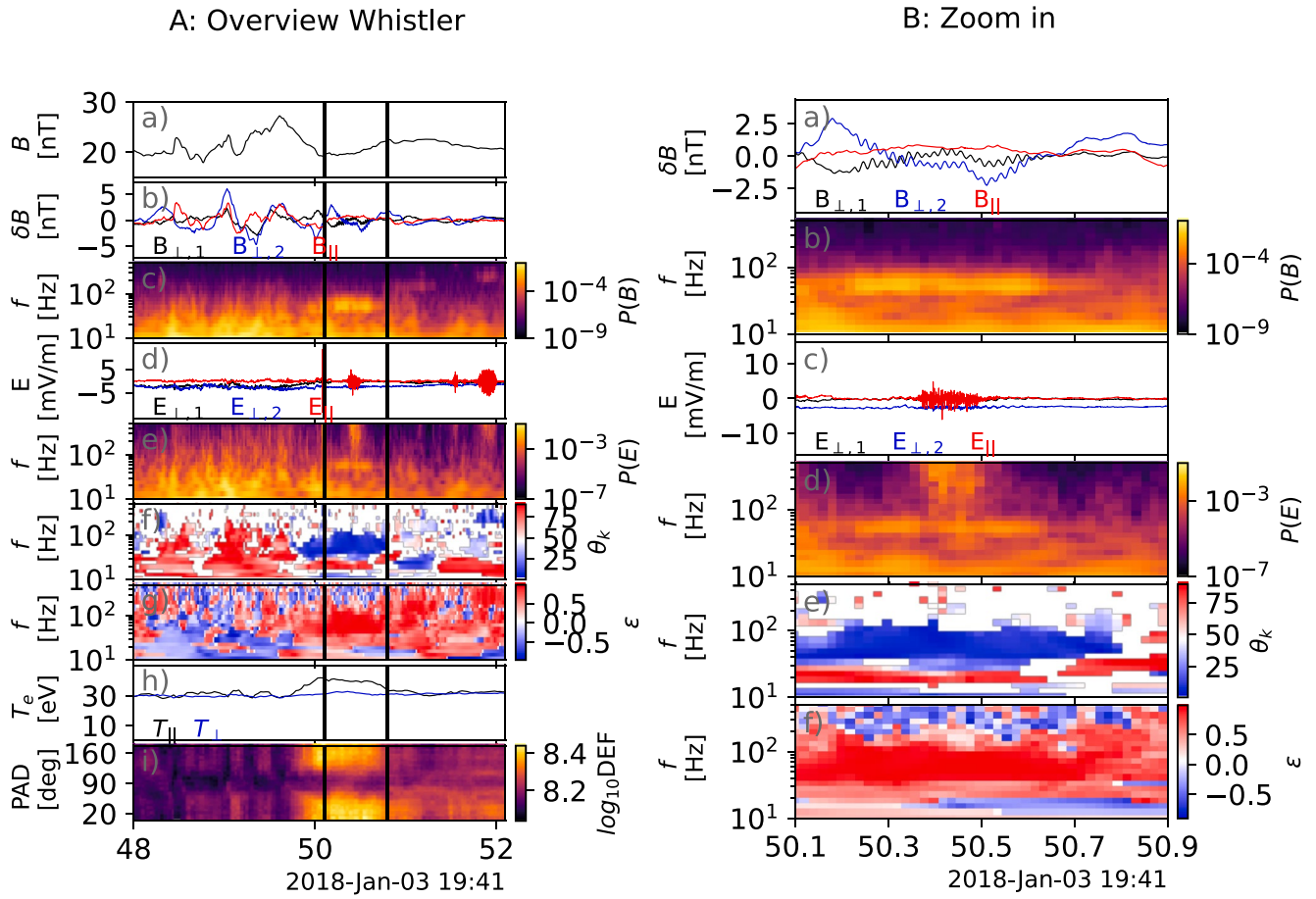

Figure 3. Example of whistler waves observed inside the jet. A: (a) Magnetic field magnitude $|B|$, (b) AC magnetic field $\delta\vec{B}$ in field aligned coordinate (FAC), (c) magnetic field spectrum $P(B)$ in units of [(nT)^2/Hz], (d) electric field $\vec{E}$ in FAC, (e) electric field spectrum $P(E)$ in units of [(mV/m)^2/Hz], (f) propagation angle θ_k, (g) ellipticity ϵ, and (h) parallel and perpendicular electron temperatures $T_{e,\parallel}$, $T_{e,\perp}$, (i) average electron pitch angle distribution in units of [kev/(cm^2 s sr keV)]. The vertical black lines indicate the time interval for B. B: (a) AC magnetic field $\delta\vec{B}$ in FAC, (b) magnetic field spectrum $P(B)$ in units of [(nT)^2/Hz], (c) electric field $\vec{E}$ in FAC, (d) electric field spectrum $P(E)$ in units of [(mV/m)^2/Hz], (e) propagation angle θ_k, (f) ellipticity ϵ.

Right handed, circularly polarized electromagnetic waves that have a small propagating angle with respect to the magnetic field are typical properties of whistler waves. Whistler waves in the magnetosheath, sometimes also referred to as lion roars, were first reported by Smith et al. (1969) and have been repeatedly reported together with mirror mode waves (Breuillard et al., 2018; Tsurutani et al., 1982). Whistler waves in magnetosheath jets were already reported by Gunell et al. (2014) and confirmed by Karlsson et al. (2018). However, their generation mechanism has not yet been investigated.

Gunell et al. (2014) suggested that electric fields at the boundary of jets can accelerate electrons to form beams. These beams can then excite whistler waves through Cherenkov resonances (Stenzel, 1999). However, our data does not show an increased electric field close to the jet boundary, but we cannot rule out the existence of an electron beam. An electron beam might not be observed since the FPI instrument does not resolve electrons below 10 eV which corresponds to an electron speed ≈1,800 km s^{-1}.

Thorne and Tsurutani (1981) suggested that whistler mode waves in the magnetosheath are generated from the cyclotron resonance instability for anisotropic electron temperatures with $T_{e\parallel} < T_{e\perp}$. However, whistler waves in the magnetosheath have also been observed for butterfly-shaped pitch-angle distribution even though $T_{e\parallel} > T_{e\perp}$ (Svenningsson et al., 2022). These whistler waves were also associated with magnetic field minima. A study by Breuillard et al. (2018) reported observation of whistler waves that were generated through the ion cyclotron resonance even though $T_{e,\parallel} > T_{e\perp}$. The authors also reported that the whistler waves are often embedded in the

local minima of mirror mode waves. They suggested that a perpendicular temperature anisotropy ($T_{e\parallel} < T_{e\perp}$) in a particular energy range can generate whistler waves.

Svenningsson et al. (2022) found whistler waves in the magnetosheath in regions stable to the previous described instability. These whistler waves are found inside ion-scaled local magnetic minima and are associated with butterfly-shaped electron pitch-angle distributions. The instability of a butterfly-shaped electron pitch-angle distribution with respect to whistler waves was confirmed with modeling. While the authors focused on the quasi-parallel magenotsheath, similar observations have been made in the quasi-perpendicular magnetosheath inside local magnetic minima of mirror mode structures (Kitamura et al., 2020). The whistler waves inside the jet were observed during a local magnetic minimum and the electron pitch-angle distribution is butterfly-shaped. This points toward a generation of the whistler waves through a butterfly-shaped pitch-angle distribution.

We can confirm the existence of whistler waves in magnetosheath jets in agreement with previous work (Gunell et al., 2014; Karlsson et al., 2018), but we suggest that the waves are most likely generated by a butterfly-shaped pitch-angle distribution in local magnetic minima. The butterfly-shaped pitch angle distribution was also present during the other occurrences of whistler waves in the same jet (data not shown). The remaining open question is what causes such butterfly-shaped pitch angle distributions. Yao et al. (2018) found that butterfly pitch-angle distribution were created by betatron cooling inside mirror modes. Svenningsson et al. (2022) suggested that butterfly pitch-angle distribution can have other sources such as discontinuities or current sheets. Since we were not able to classify the 1 Hz waves we cannot determine which of the named processes are important for forming a butterfly-shaped pitch-angle distributions inside of jets.

Note, the longest lasting whistler packet is observed between 19:42:10–19:42:15 UT (Figures 1Bj–1Bm), which is outside the jet. In comparison to the previous discussed packet, it is not associated with 1 Hz waves. This points to another generation mechanism for this packet, or the wave propagated there, but was generated elsewhere. As this packet lies outside the jet, it will not be discussed further here.

3.3. Broadband Electrostatic Waves

Several wave packets of electrostatic waves inside the jet can be observed in the electric field as seen in Figure 1Bc. We will investigate and discuss one of these wave packets which was observed between 19:41:51.8–51.9 UT in more detail to determine the nature of these waves. Figure 4A gives an overview over the AC magnetic field in FAC $\delta\vec{B}$ (Figure 4Aa), the electric field in FAC $\vec{E}$ (Figure 4Ab), and their spectra $P(E)$ and $P(B)$ (Figures Ac and Ad). Figure 4B shows the electric field measurements parallel to the magnetic field $E_{\parallel}$ from all 4 MMS spacecraft between 19:41:51.5–52.5 UT. Note, Figure 4B is a zoom-out of Figure 4A. Figure 4A shows parts of the large wave packets observed by MMS1 in Figure 4B (in black) which is also marked by the vertical lines.

The wave can only be observed in $\vec{E}$ but not in $\vec{B}$, therefore this wave is electrostatic. Furthermore, the dominating component of the electric field is $E_{\parallel}$ (Figure 4Ab). In addition, the wave forms are irregular which results in a broadband signature in $P(E)$ with frequencies around $0.2 - 2$ kHz (Figure 4Ac). Note, there is some whistler wave activity in $\delta\vec{B}$ which results in a narrow band in $P(B)$ which is not correlated with the electrostatic wave activity. The amplitude of the electrostatic wave is varying within the packet. The packet shown in Figure 4A reaches amplitudes of about 5 mV m^{-1}. The duration and amplitudes of these wave packets also vary, but generally, the duration is below 1 s (Figure 4B). The MMS 2–4 spacecraft also observed electrostatic wave activity, but the wave packets have smaller amplitudes and a different duration. Therefore, these wave packets either change their appearance quickly, are damped, or have a spatial extent, smaller than the distance between the MMS spacecrafts ($17 - 40$ km). Since we do not observe similar wave packets on multiple spacecraft, we cannot determine the propagation velocity of the electrostatic waves.

Broadband electrostatic noise (BEN) has been reported in magnetosheath jets by Karlsson et al. (2018). The authors suggested that these waves might be non-linear, solitary waves generated by ion acoustic or Langmuir waves. They were not able to investigate the wave forms since fast mode data was used in their study. Even though we also observe solitary structures (discussed in the next section), the majority of the broadband signatures in the electric field spectra can be linked to localized wave packets in the electric field and not solitary waves.

The properties of the above described waves agree with properties of the ion acoustic wave mode. Ion acoustic waves are electrostatic waves showing fluctuations parallel to the magnetic field, propagating parallel to the

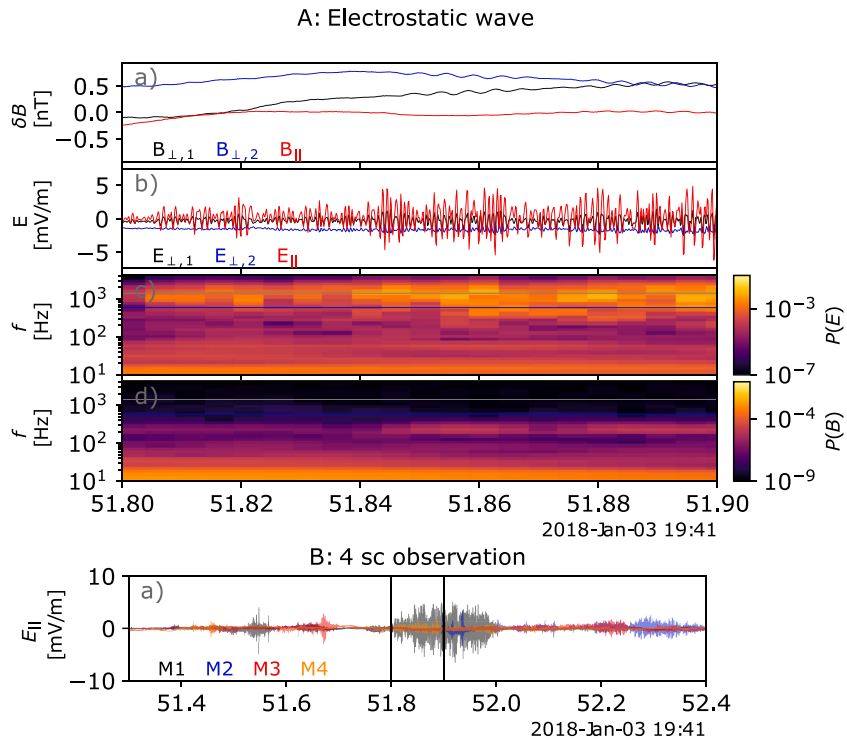

Figure 4. Example of an broadband electrostatic wave. A: MMS1 observations: (a) AC magnetic field $\delta\vec{B}$ in field aligned coordinate (FAC), (b) electric field $\vec{E}$ in FAC, (c) electric field spectrum $P(E)$ in units of $[(\mathrm{mV/m})^2/\mathrm{Hz}]$, (d) magnetic field spectrum $P(B)$ in units of $[(\mathrm{nT})^2/\mathrm{Hz}]$, B: four spacecraft observation of parallel electric field $E_{\|}$. In the spectra (c, d) the gray line indicates the ion plasma frequency f_{pi} and the blue line indicates the electron cyclotron frequency f_{ce}. The vertical black line indicates the time interval of A.

magnetic field with frequencies both above and below the ion plasma frequency $f_{\mathrm{pi}} \approx 1.5$ kHz. However, ion acoustic waves are heavily damped if $T_e < T_i$ which is generally the case in the magnetosheath as well as during the jet observation (not shown). Unless they are locally generated and strongly driven, it is not expected that ion acoustic waves propagate far in the magnetosheath. Therefore, it is unlikely that these broadband electrostatic waves are ion acoustic wave modes.

Another possibility are Bernstein modes, since they are also electrostatic. However, they are usually observed at harmonics of the ion cyclotron ($f_{ci} \approx 0.3$ Hz) or electron cyclotron ($f_{ce} \approx 600$ Hz) frequencies. The observed frequency range does not correspond to ion Bernstein modes. Furthermore, we cannot observe banded emission at multiples of the electron cyclotron frequency but a broadband signature. Therefore, it is unlikely that these waves are electron Bernstein waves.

Shin et al. (2005) suggested that an electron acoustic mode could explain the electrostatic waves between the electron gyrofrequency ($f_{ce} \approx 600$ Hz) and the ion plasma frequency ($f_{pi} \approx 1{,}500$ Hz). The authors studied the electron velocity distribution while they observed such electrostatic wave activity. They found that two electron distributions, one cold, beam-like distribution and one warm, background distribution can drive an electron acoustic mode. In addition, Shin et al. (2007) found that electrostatic quasi-monochromatic waves are most often observed close to the bow shock. This was linked to the shock potential at the bow shock that accelerates electrons which then form a beam-like component. We cannot observe a cold electron beam due to the limitations of the MMS FPI instrument. Therefore, we cannot rule out that such a cold beams exists as the driver for these waves. In addition, the maximum intensity of our observed waves is below $f_{pi} \approx 1{,}500$ Hz which could fit the criteria for electron acoustic modes according to Shin et al. (2005).

Gary (1987) performed an analysis of electron acoustic waves, computing growth rates and stability thresholds for the electron/electron acoustic and the electron/ion acoustic instabilities. In the former a cold electron population has a relative drift speed to the warm electron distribution, and the ions do not matter for the instability. In

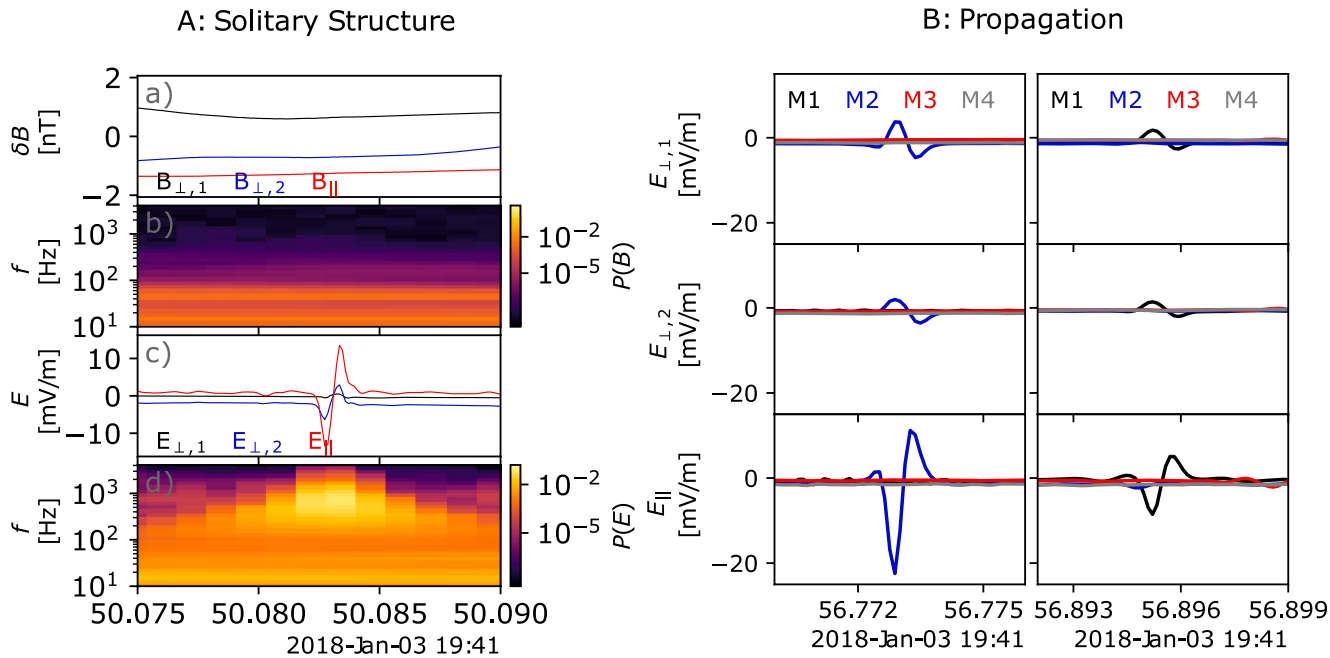

Figure 5. Example of an electrostatic solitary wave. A: MMS1 observation: (a) AC magnetic field $\delta\vec{B}$ in field aligned coordinate (FAC), (b) magnetic field spectrum $P(B)$ in units of [(nT)^2/Hz], (c) electric field $\vec{E}$ in FAC, (d) electric field spectrum $P(E)$ in units of [(mV/m)^2/Hz]. B: MMS1-4 observations: Electric field $\vec{E}$ components in FAC with 120 ms time difference. Panels A and B show two different events.

the latter case the cold electrons drift also with respect to the ions. In our case, a cold electron population with $k_B T_{e,c} \approx 1$ eV carrying 10% of the total electron density and drifting at $v \approx 5 v_{th,c}$ with respect to a warm electron background at $k_B T_{e,w} \approx 30$ eV would be consistent with the electron measurements, as we do not have access to the lowest energy part of the distribution. This distribution function would be unstable to both the electron/electron acoustic and electron/ion acoustic instabilities (Gary, 1987). However, since the threshold for the electron/ion acoustic instability is lower, that is the most likely instability to occur. The electron/ion acoustic instability also allows lower relative drift speeds and is consistent with the maximum wave intensity being observed below the ion plasma frequency.

We come to the conclusion that these waves are most likely electron acoustic mode waves. We cannot confirm nor rule out their generation mechanism with an cold electron beam due to limitations of the available instruments.

3.4. Electrostatic Solitary Waves

In Figure 1Bc we do not only observe wave packets of electrostatic waves, but also solitary waves. Here we show three occurrences of solitary waves. The solitary wave with highest amplitude observed by the MMS1 spacecraft is observed around 19:41:50 UT and will be investigated in more detail in the following. An overview over the observation of this solitary wave is given in Figure 5A between 19:41:50.075–50.090 UT.

The solitary wave in Figure 5A reaches an amplitude of about 12 mV m^{-1} and has a duration of about 1.5 ms. The highest fluctuation can be observed in $E_\parallel$ while fluctuations in $E_\perp$ are much smaller. $\delta\vec{B}$ does not show any fluctuations, therefore this is an ESW. The bipolar pulse causes a broadband structure in the spectrum. In addition, small amplitude precursors are visible in the parallel electric field.

In Figure 5B another example of an ESW is shown which was observed by the MMS2 spacecraft 19:41:56.774 UT. As in the previous example, the duration is about 2 ms and the largest variation is observed in $E_\parallel$. The amplitude of the negative peak is about 20 mV m^{-1}. In addition, there is also a small positive peak before the large bipolar variation. Approximately 120 ms later a similar signature was observed by the MMS1 spacecraft with a much smaller amplitude.

The presented ESW show first a negative and then a positive electric field variation in $E_{\parallel}$. The electric potential can be used to classify ESWs. Electron phase space holes have a positive potential and ion phase space holes have a negative potential. In order to determine the electric potential from $\vec{E}$ of the ESW, the propagation direction must be known. Single-spacecraft timing (Steinvall et al., 2022) fails, since the magnetic field (and hence the wave propagation direction) is mainly along the shorter axial probes, resulting in an unmeasurable time lag. The ESWs are not observed by all four spacecraft, so we cannot use multi-spacecraft timing to determine their velocity. However, the short duration and similar wave form between the two spacecrafts (Figure 5B) might indicated that the same ESW was first observed by MMS2 and then by MMS1. Assuming that these ESWs are the same and that they propagate parallel or anti-parallel to $\vec{B}$ we can estimate their velocity. Using a time separation of 122 ms, the speed along the magnetic field is approximately -37 km s^{-1} in the spacecraft frame. The ESW is propagating anti-parallel to the magnetic field which indicates a negative potential corresponding to an ion phase space hole. Note, this result is based on the assumption that the MMS1 and MMS2 spacecraft observe the same ESW.

Bipolar pulses in the magnetosheath have been reported before. Kojima et al. (1997) reported bipolar pulses with a duration of $1-2$ ms in the magnetosheath using the plasma wave instrument on the Geotail spacecraft. The authors suggested that electron beams could cause such ESWs in the magnetosheath. This is based on their comparison with such waves in the magnetotail where Omura et al. (1996) showed with simulations that several electron beam instabilities can cause ESWs.

A study by Graham et al. (2016) found ESWs and field-aligned electrostatic waves in the magnetosheath near the Earth's magnetopause. In the example of their study, they reported ESWs with a duration of about 1–2 ms, in between $f_{\rm pi}$ and $f_{\rm ce}$. The statistical part of their study suggested the ESWs to be electron holes generated by various instabilities, such as the beam-plasma instability, the warm bistream instability, and the electron-ion instabilities. These instabilities are caused by an additional electron population in the plasma. The ESWs reported in the study by Graham et al. (2016) have a similar to the one described above. This suggests that the ESWs found inside the jet might be related to electron phase space holes rather than ion phase space holes.

A study by Pickett et al. (2003) used the Cluster spacecraft and reported similar bipolar signatures that have an duration of $25-100\,\mu$s in the magnetosheath. Cluster's Wideband Plasma Wave Receiver with a lower frequency cutoff at 1 kHz was used for the study. The Wideband Plasma Wave Receiver cannot detect pulses with a duration longer than 2 ms. At the same time, the MMS EDP instrument is sampled with a frequency of 8 kHz, and therefore no pulses with a duration longer than $\approx$0.25 ms are detected with this instrument. It cannot be ruled out that these are the same phenomena at different frequencies due to different limitations of the respective instruments. Pickett et al. (2005) suggested that solitary waves might be electron phase space holes in the magnetosheath. The authors observed counter-streaming electrons during electrostatic wave observation which they suggested is the source for these solitary waves.

Kojima et al. (1999) compared the pulse duration with the ion plasma oscillation period $f_{\rm pi}^{-1}$ and the electron plasma oscillation period $f_{\rm pe}^{-1}$ in different regions. They found that if these times are comparable it suggests whether ion or electron dynamics play an important role. In our case, the ESWs have a duration of approximately 1.5 ms which is comparable to the ion plasma oscillation period $f_{\rm pi}^{-1} \approx 0.6$ ms. This suggests that ion dynamics are more relevant for the observed solitary structure which is in conflict with the results of Graham et al. (2016).

For the first time we reported ESWs inside a jet. These ESWs can only be observed in burst mode due to their short duration of approximately 1–2 ms since the electric field is sampled with 32 Hz in fast mode. Since previous studies of waves in jets used lower resolution data they were not able to resolve such short-lived structures. The observed ESWs have a small spatial extent or are heavily damped, since they are only observed by one or two spacecraft and not all four. Based on the timing analysis and the assumption that the MMS1 and MMS2 spacecraft see the same ESW, we find that one of the ESWs is an ion phase space hole. However, further analysis would be needed to confirm this result. We were not able to determine the source of these ESWs.

3.5. Wave Modes in the Frequency Range 5–200 Hz

So far, we have discussed 1 Hz waves, whistler waves, broadband electrostatic waves and ESWs. But, Figures 1Bj and 1Bk shows wave activity up to the ion cyclotron frequency (gray line) in the electric spectrum $P(E)$ and the magnetic field spectrum $P(B)$ which cannot be explained by the above presented wave modes. We therefore investigate the electric and magnetic field activity in FAC in the frequency range 5–200 Hz. The frequency range

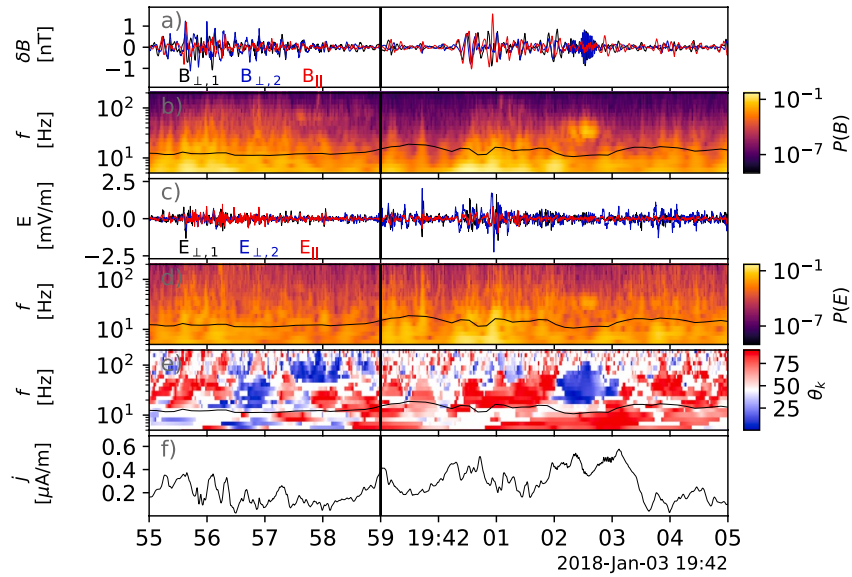

Figure 6. Wave activity between 5 and 200 Hz. (a) AC magnetic field $\delta\vec{B}$ in field aligned coordinate (FAC), (b) magnetic field spectrum $P(B)$ in units of [(nT)^2/Hz], (c) electric field $\vec{E}$ in FAC, (d) electric field spectrum $P(E)$ in units of [(mV/m)^2/Hz], (e) propagation angle θ_k, (f) the magnitude of the current density j. The black line in the spectra (b, d, e) indicates the lower hybrid frequency $f_{\rm lh}$. The vertical line marks the end of the jet time interval.

was chosen such that the influence from the 1 Hz waves as well as the electrostatic waves are suppressed. Figure 6 gives an overview over the wave activity in the frequency range 5–200 Hz between 19:41:55–42:05 UT. Figure 6a shows the band-pass filtered AC magnetic field $\delta\vec{B}$ in FAC in the frequency range 5–200 Hz and Figure 6b shows the corresponding spectrum. Figure 6c shows the band-pass filtered electric field $\vec{E}$ in FAC in the frequency range 5–200 Hz and Figure 6d shows the corresponding spectrum $P(E)$. In Figure 6e the propagation angle θ_k is shown and Figure 6f shows the current density j.

Figures 6a–6e shows that wave activity in the frequency range 5–200 Hz is present throughout the entire interval. Note, whistler waves are observed in this time range and they can be identified by their low propagation angle θ_k (e.g., 19:42:02–03 UT). However, they do not account for all the observed wave activity. Since we have already discussed whistler waves, we will now focus on the remaining wave activity. By comparing $P(B)$ (Figure 6b) and $P(E)$ (Figure 6d) it is clear that there is both electromagnetic wave activity and electrostatic wave activity. The waves in $\delta\vec{B}$ reach amplitudes up to 1 nT (Figure 6a) and waves in $\vec{E}$ reach amplitudes of about 2 mV m^{-1} (Figure 6c). The frequency of the waves spans the entire investigated frequency range from 5 to 200 Hz. The wave forms are irregular and not well defined, which leads to a broadband signatures in the respective spectra. The wave activity is increased below the lower hybrid frequency $f_{\rm lh}$ (indicated by the black lines in Figures 6b, 6d, and 6e) and decreases with increasing frequency (Figures 6b and 6d). This observation is more pronounced in $P(B)$ (Figure 6b) in comparison to $P(E)$ (Figure 6d). The propagation angle θ_k (Figure 6e) suggests that the propagation angle is close to perpendicular ($\theta_k \approx 90°$) with respect to $\vec{B}$ for waves below approximately 100 Hz.

The packet between 19:41:55–58 UT shows variations both in $\vec{E}$ and $\delta\vec{B}$ and all electric and magnetic field components show wave activity (Figures 6a and 6c). The wave packets between 19:41:59-42:00 UT and 19:42:03–03 UT show only low amplitude wave activity in $\delta\vec{B}$ and most activity in $E_\perp$. The packet between 19:42:00–02 UT shows wave activity in both the electric as well as the magnetic field, but the variations are dominantly in $E_\perp$.

Lower hybrid frequency waves are electrostatic waves with frequencies close to the lower hybrid frequency $f_{\rm lh}$, given through the relation $f_{\rm lh}^{-2} = \left(f_{\rm ci}^2 + f_{\rm pi}^2\right)^{-1} + (f_{\rm ci} f_{\rm ce})^{-1}$, where $f_{\rm ci}$ is the proton gyrofrequeny, $f_{\rm ce}$ is the electron gyrofrequency, and $f_{\rm pi}$ is the ion plasma frequency. Lower hybrid frequency waves have fluctuations mainly in $E_\perp$ and propagate perpendicular to $\vec{B}$. Even though, lower hybrid waves are considered to be electrostatic, they have been associated with magnetic field fluctuations. These fluctuations are associated with currents generated by the wave (Norgren et al., 2012) which are mainly observed in $B_\parallel$. The lower hybrid mode is found on the same dispersion surface as the whistler, the fast magnetosonic or the compressional Alfvén mode (André, 1985). For

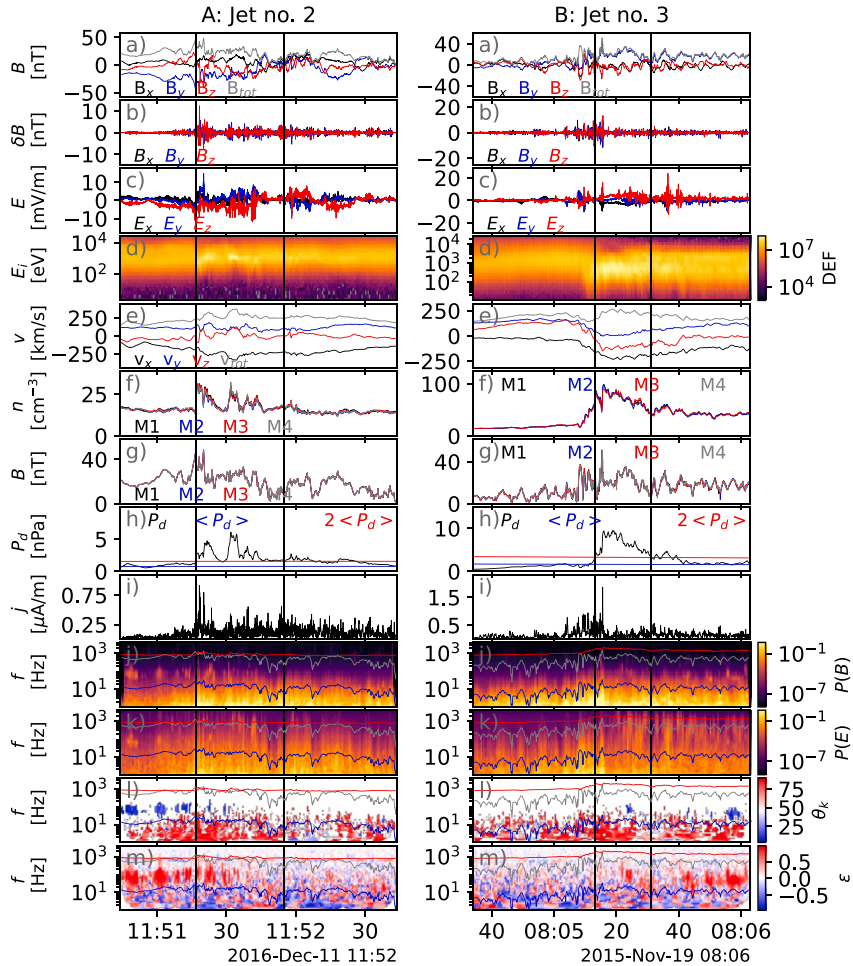

Figure 7. Same as Figure 1B for jet 2 and jet 3.

more oblique propagation angles the properties of the waves are different and an electromagnetic, right circularly polarized mode would be generated instead. Different propagation angles of the waves due to varying plasma conditions could cause different wave properties. The wave packets after 19:41:59 UT are associated with properties of a lower hybrid waves. The packet from 19:41:55–58 UT does in addition show fluctuations in $B_{\perp}$ and in $E_{\parallel}$ which do not correspond to typical properties of lower hybrid waves.

Gunell et al. (2014) reported wave activity in the lower frequency range which was confirmed by Karlsson et al. (2018). Gunell et al. (2014) suggested that these waves are generated by currents that develop near the jet boundaries. In Figures 1Bi and 6f an increase in the current density can be observed during increased wave activity. This suggests that these waves are likely generated by currents. In this case the currents could develop from the rotation of the magentic field. But, in general, any change in the magnetic field causes a current to develop.

We observe increased wave activity between 5 and 200 Hz. Some wave packets are consistent with lower hybrid waves while other wave packets are more electromagnetic. We suggest that these waves are of the same mode and the electrostatic approximations for lower hybrid waves is an approximation that does not account for all observed waves.

4. Observations of Waves in Other Jets

In this section wave activity in two more jets is presented and compared to the previous findings. One of the jets was observed on 2016-12-11 11:51:17–55 UT, an overview of the available burst mode data is given in Figure 7A. We will refer to this jet as jet 2. The other one, referred to as jet 3, was observed on 2015-11-19

Table 1
Observed Waves in Jet 1, Jet 2, and Jet 3

Wave/Jet	Jet 1 2018-January-03	Jet 2 2016-December-11	Jet 3 2015-November-19
0.2 Hz	–	11:51–12:03	07:55–8:15
1 Hz	19:42:47–51	11:51:15–25	08:05:20–30
Whistler	19:41:50.2–50.7	11:51:22.8–23.6	08:05:23.3–23.7
e-acoustic	19:41:51.8–51.9	11:51:41.5–41.8	08:05:24.25–24.45
ESW	19:41:50.08–50.09	–	–
5–200 Hz	19:41:55–42:05	11:51:52–52:01	08:05:07–17

Note. The indicated times correspond to the times used for the figures showing examples of the respective wave.

08:05:13–31 UT and the overview is shown in Figure 7B. From now on we will refer to the jet that was described in detail in the previous section as jet 1.

The jets were chosen such that they were observed in different magnetosheath regions under different conditions. Jet 1 was observed on the flank of the magnetosheath behind the quasi-perpendicular bow shock. Jet 2 was observed behind the quasi-perpendicular bow shock in the subsolar magnetosheath. Jet 3 was observed behind the quasi-parallel bow shock in the subsolar magnetosheath.

In the following we will shortly report differences and similarities of the waves between these jets. An overview over all waves in jet 1–3 is presented in Table 1. We will only show the overview burst plot similar to Figure 1B in this paper. We provide all other figures, similar to the ones in the detailed analysis of jet 1, in the Supporting Information S1.

4.1. Jet 2

Jet 2 was observed on 2016-12-11 11:51:17–55 UT when the MMS spacecraft were located at $r\vec{_{GSE}} = (11.2, 4.1$ 0.9). An overview of the burst data is given in Figure 7A. This jet was located in the subsolar region ($\theta_s \approx 20°$) in the quasi-perpendicular magnetosheath with $\theta_{Bn} \approx 83°$ as explained in more detail in Section 2. Note, the dynamic pressure for this jet falls below the threshold for approximately 1.5 s around 11:51:28 UT (Figure 7Ah), for this analysis we will still consider this as a single jet. The dynamic pressure also exceeds the threshold two more times from 11:51:55–52:25 UT but with a much lower dynamic pressure. We will refer to this time interval as the trailing edge of jet 2.

The jet shows an increase in v (Figure 7Ae) as well as an increase in n_i (Figure 7Af). From Figure 7Aa showing $\vec{B}$ it becomes clear that $\vec{B}$ is highly varying. This jet shows signs of 1 Hz waves, whistler waves and broadband electrostatic waves. We used the same identification criteria as in jet 1. No ESWs were found in jet 2.

One difference in comparison to jet 1 are the properties of the whistler waves. In jet 2 the frequencies of each whistler packet are varying (Figure S3Ac in Supporting Information S1). The whistler wave packets are observed in the frequency range 30–500 Hz. The frequency within each packet is well defined. The amplitude of each whistler packet is also strongly varying and can be up to 1 nT. The observed whistler wave exists independent of the electron temperature anisotropy, both a perpendicular anisotropy $T_{e\perp} > T_{e\parallel}$ was observed as well as a parallel anisotropy $T_{e\perp} < T_{e\parallel}$ (Figure S3Ah in Supporting Information S1). The pitch angle-distribution is butterfly-shaped, similar to the observations in jet 1 (Figure S3Ah in Supporting Information S1). We suggest that the generation mechanism for the whistler waves is the same as in jet 1. The variations in the observed frequencies could be the result of variations of the local plasma properties.

Another difference are waves in $\vec{B}$ with a period around 5 s (0.2 Hz) which can be observed from 11:51 UT throughout the entire burst interval, so both inside and outside the jet (Figure 7Aa). These waves show an enhanced amplitude inside and in the trailing edge of the jet. The fast mode data of $\vec{B}$ (Figure S1A in Supporting Information S1) shows such wave activity exists both before and after the jet over at least a 10 min interval but with decrease in frequency, $f \approx 0.1$ Hz, after 11:56 UT. We will refer to this wave activity as 0.2 Hz waves. These 0.2 Hz waves are similar to the 0.1 Hz waves reported by Karlsson et al. (2018). We could not determine whether these waves are locally produced or ULF waves generated in the foreshock and convected into the magnetosheath as suggested by Karlsson et al. (2018). Since these waves are present both inside and outside the jet we do not investigate these waves in more detail.

Jet 2 shows similar wave activity as jet 1. Jet 2 is also associated with 1 Hz waves, whistler waves, electron acoustic waves, and waves around the lower hybrid frequency. In contrast to jet 1, we could not detect ESWs in jet 2. There is additional wave activity in the magnetic field with a frequency of 0.2 Hz. We could not find any indication that the waves are generated differently in jet 2 compared to the waves in jet 1.

4.2. Jet 3

Jet 3 was observed on 2015-11-19 08:05:13–31 UT when the spacecraft were located at $\vec{r_{GSE}} = (11.8, 2.3, -0.9)$. The burst overview is given in Figure 7B. Note, the actual available burst interval starts 90 s earlier. In order to get a better overview of the jet we chose to show a shortened time interval of burst data. This jet was located in the subsolar region ($\theta_s \approx 12°$) in the quasi-parallel magnetosheath with $\theta_{bn} \approx 39°$. As in jet 2 we define the trailing the edge of the jet from 08:05:31–40 UT as the dynamic pressure exceeds the threshold three more times.

The jet shows, as jet 1 and 2, an increase in $\vec{v}$ (Figure 7Be) and in n_i (Figure 7Bf). The jet is observed after an increase in $|\vec{B}|$ (Figure 7Ba). There is an increase in wave activity during the jet and during the trailing edge in both the electric field $\vec{E}$ (Figures 7Bc and 7Bk) and $\delta\vec{B}$ (Figures 7Bb and 7Bj). We were able to detect 1 Hz waves, whistler waves, broadband electrostatic waves, and waves between 5 and 200 Hz. No ESWs were observed in jet 3.

Jet 3 shows only one occurrence of a whistler wave which was observed around 08:05:23 UT. The amplitude of this whistler is low, approximately 0.15 nT, (Figure S8Ba in Supporting Information S1) in comparison to jet 1 and 2. During the whistler wave observation the electron temperature shows either no anisotropy or a perpendicular anisotropy $T_{e,\perp} > T_{e,\parallel}$. The pitch-angle distribution shows fewer electrons moving quasi-perpendicular to the magnetic field, but we can not identify a clear butterfly-shaped pitch-angle distribution as in jet 1 and 2 (Figure S8Aj in Supporting Information S1). Possibly, the generation mechanism the same as in jet 1 and 2, but the signature of the butterfly-shaped pitch-angle distribution is weaker causing whistler waves with a smaller amplitude.

Figure 7Ba shows waves with a period of about 0.2 Hz similar to jet 2. This wave activity can also be observed in the fast magnetic field data (S6A) over an extended period of time before and after the jet.

Jet 3 shows similar wave activity as jet 1 and jet 2. Jet 3 is associated with 1 Hz waves, whistler waves, electron acoustic waves, and waves around the lower hybrid frequency. We suggest that the generation mechanisms are the same as in the other two jets. In contrast to jet 1, we did not observe ESWs in jet 3. As in jet 2, we observe 0.2 Hz waves in jet 3.

5. Conclusion and Outlook

We have investigated wave activity inside, and in the vicinity of, three different magnetosheath jets. We find 1 Hz waves (1), whistler waves (2), electron acoustic waves (3), waves around the lower hybrid frequency (4), ESWs (5), and 0.2 Hz waves (6). Of these waves, (1), (2), (3), and (4) were observed in all three jets. ESWs were only observed in jet 1. The 0.2 Hz waves in the magnetic field were only observed in jet 2 and jet 3. For these waves have made the following findings:

1. 1 Hz waves are electromagnetic waves associated with density and magnetic field gradients. These waves show properties similar to mirror mode waves, slow-mode waves, and electromagnetic ion cyclotron waves. The associated density and magnetic field gradients suggest that this wave mode cannot be associated with a basic wave mode as it is derived assuming a homogeneous plasma. We report this wave mode for the first time in magnetosheath jets.
2. Whistler waves: The observation of whistler waves is in agreement with previous work by Gunell et al. (2014) and Karlsson et al. (2018). We find that whistler waves are likely to be excited by a butterfly-shaped pitch-angle distribution while Gunell et al. (2014) suggested a generation through electron beams.
3. Electron acoustic waves have a broadband signature in the electric field and can therefore be described as BENs. We suggest that the electron acoustic waves are generated by an additional cold electron population. In contrast, Karlsson et al. (2018) proposed an association with either Langmuir waves or ion acoustic waves.
4. Lower hybrid waves: Wave activity close the lower hybrid frequency which is in agreement with Gunell et al. (2014) and Karlsson et al. (2018). Some of these lower hybrid waves show strong electromagnetic properties. These waves are most likely generated due to increased currents flowing inside, and in the vicinity of, the jet caused by changes in magnetic field orientation or magnitude.
5. ESWs: We report ESWs inside jets for the first time. We found that one of the observed ESWs might be an ion phase space hole, however further investigations are needed to confirm this result. Even though they cause broadband electric field signatures they can not be accounted for majority of BEN in contrast to what was suggested by Karlsson et al. (2018).

6. 0.2 Hz waves can be observed in the magnetic field with a period of 5 s, both inside and outside of jet 2 and jet 3. Similar oscillations with a period of 10 s have been reported by Karlsson et al. (2018), but only in the quasi-parallel magnetosheath. In contrast, jet 2 was observed in the quasi-perpendicular magnetosheath.

Identifying waves in magnetosheath jets can be challenging since magnetosheath jets are associated with density and magnetic field gradients. Properties of basic wave modes are derived using approximations of linearity and homogeneity, the validity of these approximations needs to be verified in the context of magnetosheath jets. Especially for low frequency waves, these assumptions are often violated as they are on time scales similar to density and magnetic field changes. In addition, for these low frequency waves the magnitude of the variations becomes comparable to the background magnetic field. This challenges the assumption on the linearity of the wave modes.

An additional challenge are limitations due to instruments. For the electron distribution, a better temporal resolution would be favorable to study high frequency phenomena such as broadband electrostatic waves and solitary structures. In addition, the MMS FPI instrument only resolves electrons above 10 eV. In the magnetosheath we would expect to see electron beams with lower energies.

The investigated jets were located in different regions of magnetosheath behind both the quasi-parallel and quasi-perpendicular bow shock. Only jet 1 shows signatures of solitary waves but did not show 0.2 Hz waves in the magnetic field as jet 2 and jet 3. A statistical study is needed to determine under which conditions the waves are observed. 1 Hz waves, whistler waves, electron acoustic waves, and waves around the lower hybrid frequency are consistently observed in our three jets, independent of their location or the magnetosheath conditions.

An increased wave activity inside, and in the vicinity of, jets reflects the complicated interaction of different plasma environments. Furthermore, waves can transfer energy between particle populations inside jets as well as at the boundary of the jet interacting with the surrounding magentosheath plasma. Waves can shed light on the evolution of jets as they propagate through the magnetosphere and potentially interact with the magnetosphere through the magnetopause. Especially the 1 Hz electromagnetic waves which develop at the boundary of jets could transfer energy from the plasma population inside the jet to the surrounding magnetosheath plasma. This would affect the evolution of the jet by slowing it down and decreasing the energy of the plasma inside the jet. Further investigations are needed to calculate the Poynting flux to determine in the direction of the energy transfer. Currents that drive lower hybrid waves could form at the boundaries of jets due to changes in the magnetic field. The energy to drive these lower hybrid waves could come from the kinetic energy or the thermal energy of the particles. A more in depth analysis would be needed to identify the source of the energy which is outside the scope of this work. An additional source for the lower hybrid waves could be 1 Hz waves associated with their large magnetic field amplitudes which could drive currents that generate waves in the lower hybrid frequency range. Whistler waves are know to contribute to the heating of electrons (Breuillard et al., 2018) and could therefore be associated with an increase in the electron temperature inside magnetosheath jets. If electron heating due to whistler waves can be observed in magnetosheath jets is subject to further research.

In the future, a statistical study of waves in, and in the vicinity of, jets could reveal systematical differences between jets. Differences in wave activity could shed light on differences in the internal structure. Furthermore, the use of simulations can help to understand and predict properties of waves in non-linear and inhomogeneous environments better. Studying wave activity in magnetosheath jets is a step toward understanding the microphysics of these jets which can help to gain knowledge about their evolution and formation.

Data Availability Statement

We acknowledge the use of MMS data available under https://lasp.colorado.edu/mms/sdc/public/. We acknowledge use of NASA/GSFC's Space Physics Data Facility's OMNIWeb service, and OMNI data available at https://omniweb.gsfc.nasa.gov/. Data analysis was performed using the pyspedas package available at https://github.com/spedas/pyspedas, the pytplot package available at https://github.com/MAVENSDC/PyTplot, and the IRFU-Matlab analysis package available at https://github.com/irfu/irfu-matlab. This research made use of PlasmaPy version 0.7.0, a community-developed open source Python package for plasma research and education (PlasmaPy Community et al., 2021).

Acknowledgments
The authors would like to thank Ida Svenningsson for useful discussions. E. Krämer and M. Hamrin were supported by Vetenskapsrådet (VR) dnr 2018-03623. H. Gunell was supported by the Swedish National Space Agency (SNSA) Grant 108/18. O. Goncharov was supported by the Czech Science Foundation under Contract 21-26463S. T. Karlsson acknowledges the support of the Swedish National Space Agency (SNSA, Grant 90/17). Mats André was supported by the Swedish National Space Agency contract SNSA 2020-00058.

References

André, M. (1985). Dispersion surfaces. *Journal of Plasma Physics*, *33*(1), 1–19. https://doi.org/10.1017/s0022377800002270
Archer, M., & Horbury, T. (2013). Magnetosheath dynamic pressure enhancements: Occurrence and typical properties. *Annales Geophysicae*, *31*(2), 319–331. https://doi.org/10.5194/angeo-31-319-2013
Blanco-Cano, X., Preisser, L., Kajdič, P., & Rojas-Castillo, D. (2020). Magnetosheath microstructure: Mirror mode waves and jets during southward IP magnetic field. *Journal of Geophysical Research: Space Physics*, *125*(9), e27940. https://doi.org/10.1029/2020JA027940
Breuillard, H., Le Contel, O., Chust, T., Berthomier, M., Retino, A., Turner, D., et al. (2018). The properties of lion roars and electron dynamics in mirror mode waves observed by the magnetospheric multiscale mission. *Journal of Geophysical Research: Space Physics*, *123*(1), 93–103. https://doi.org/10.1002/2017ja024551
Burch, J., Moore, T., Torbert, R., & Giles, B. (2016). Magnetospheric multiscale overview and science objectives. *Space Science Reviews*, *199*(1), 5–21. https://doi.org/10.1007/s11214-015-0164-9
Dunlop, M., Southwood, D., Glassmeier, K.-H., & Neubauer, F. (1988). Analysis of multipoint magnetometer data. *Advances in Space Research*, *8*(9–10), 273–277. https://doi.org/10.1016/0273-1177(88)90141-x
Eastwood, J., Lucek, E., Mazelle, C., Meziane, K., Narita, Y., Pickett, J., & Treumann, R. (2005). The foreshock. *Space Science Reviews*, *118*(1), 41–94. https://doi.org/10.1007/s11214-005-3824-3
Ergun, R., Tucker, S., Westfall, J., Goodrich, K., Malaspina, D., Summers, D., et al. (2016). The axial double probe and fields signal processing for the mms mission. *Space Science Reviews*, *199*(1), 167–188. https://doi.org/10.1007/s11214-014-0115-x
Formisano, V. (1979). Orientation and shape of the Earth's bow shock in three dimensions. *Planetary and Space Science*, *27*(9), 1151–1161. https://doi.org/10.1016/0032-0633(79)90135-1
Gary, S. P. (1987). The electron/electron acoustic instability. *Physics of Fluids*, *30*(9), 2745–2749. https://doi.org/10.1063/1.866040
Gary, S. P. (1992). The mirror and ion cyclotron anisotropy instabilities. *Journal of Geophysical Research*, *97*(A6), 8519–8529. https://doi.org/10.1029/92ja00299
Gary, S. P., Fuselier, S. A., & Anderson, B. J. (1993). Ion anisotropy instabilities in the magnetosheath. *Journal of Geophysical Research*, *98*(A2), 1481–1488. https://doi.org/10.1029/92ja01844
Goncharov, O., Gunell, H., Hamrin, M., & Chong, S. (2020). Evolution of high-speed jets and plasmoids downstream of the quasi-perpendicular bow shock. *Journal of Geophysical Research: Space Physics*, *125*(6), e2019JA027667. https://doi.org/10.1029/2019JA027667
Graham, D. B., Khotyaintsev, Y. V., Vaivads, A., & André, M. (2016). Electrostatic solitary waves and electrostatic waves at the magnetopause. *Journal of Geophysical Research: Space Physics*, *121*(4), 3069–3092. https://doi.org/10.1002/2015JA021527
Gunell, H., Stenberg Wieser, G., Mella, M., Maggiolo, R., Nilsson, H., Darrouzet, F., et al. (2014). Waves in high-speed plasmoids in the magnetosheath and at the magnetopause. *Annales Geophysicae*, *32*(8), 991–1009. https://doi.org/10.5194/angeo-32-991-2014
Hasegawa, A. (1969). Drift mirror instability in the magnetosphere. *The Physics of Fluids*, *12*(12), 2642–2650. https://doi.org/10.1063/1.1692407
Huang, S., Sahraoui, F., Yuan, Z., Le Contel, O., Breuillard, H., He, J., et al. (2018). Observations of whistler waves correlated with electron-scale coherent structures in the magnetosheath turbulent plasma. *The Astrophysical Journal*, *861*(1), 29. https://doi.org/10.3847/1538-4357/aac831
Hurtig, T., Brenning, N., & Raadu, M. A. (2005). The role of high frequency oscillations in the penetration of plasma clouds across magnetic boundaries. *Physics of Plasmas*, *12*(1), 012308. https://doi.org/10.1063/1.1812276
Karlsson, T., Plaschke, F., Hietala, H., Archer, M., Blanco-Cano, X., Kajdič, P., et al. (2018). Investigating the anatomy of magnetosheath jets - MMS observations. *Annales Geophysicae*, *36*(2), 655–677. https://doi.org/10.5194/angeo-36-655-2018
Kennel, C. F., & Petschek, H. (1966). Limit on stably trapped particle fluxes. *Journal of Geophysical Research*, *71*(1), 1–28. https://doi.org/10.1029/jz071i001p00001
Kitamura, N., Omura, Y., Nakamura, S., Amano, T., Boardsen, S., Ahmadi, N., et al. (2020). Observations of the source region of whistler mode waves in magnetosheath mirror structures. *Journal of Geophysical Research: Space Physics*, *125*(5), e2019JA027488. https://doi.org/10.1029/2019ja027488
Kivelson, M. G., & Russell, C. T. (1995). *Introduction to space physics*. Cambridge University Press.
Kojima, H., Matsumoto, H., Chikuba, S., Horiyama, S., Ashour-Abdalla, M., & Anderson, R. R. (1997). Geotail waveform observations of broadband/narrowband electrostatic noise in the distant tail. *Journal of Geophysical Research*, *102*(A7), 14439–14455. https://doi.org/10.1029/97JA00684
Kojima, H., Matsumoto, H., & Omura, Y. (1999). Electrostatic solitary waves observed in the geomagnetic tail and other regions. *Advances in Space Research*, *23*(10), 1689–1697. https://doi.org/10.1016/S0273-1177(99)00377-4
Krall, N. A., & Liewer, P. C. (1971). Low-frequency instabilities in magnetic pulses. *Physical Review A*, *4*(5), 2094–2103. https://doi.org/10.1103/physreva.4.2094
Le Contel, O., Leroy, P., Roux, A., Coillot, C., Alison, D., Bouabdellah, A., et al. (2016). The search-coil magnetometer for mms. *Space Science Reviews*, *199*(1), 257–282. https://doi.org/10.1007/s11214-014-0096-9
Lindqvist, P.-A., Olsson, G., Torbert, R., King, B., Granoff, M., Rau, D., et al. (2016). The spin-plane double probe electric field instrument for mms. *Space Science Reviews*, *199*(1), 137–165. https://doi.org/10.1007/s11214-014-0116-9
Lucek, E., Constantinescu, D., Goldstein, M., Pickett, J., Pincon, J.-L., Sahraoui, F., et al. (2005). The magnetosheath. *Space Science Reviews*, *118*(1), 95–152. https://doi.org/10.1007/s11214-005-3825-2
Norgren, C., Vaivads, A., Khotyaintsev, Y. V., & André, M. (2012). Lower hybrid drift waves: Space observations. *Physical Review Letters*, *109*(5), 055001. https://doi.org/10.1103/PhysRevLett.109.055001
Omidi, N., & Winske, D. (1995). Structure of the magnetopause inferred from one-dimensional hybrid simulations. *Journal of Geophysical Research*, *100*(A7), 11935–11955. https://doi.org/10.1029/94JA02937
Omura, Y., Matsumoto, H., Miyake, T., & Kojima, H. (1996). Electron beam instabilities as generation mechanism of electrostatic solitary waves in the magnetotail. *Journal of Geophysical Research*, *101*(A2), 2685–2697. https://doi.org/10.1029/95JA03145
Papitashvili, N. E., & King, J. H. (2020). Omni 1-min data [Dataset]. NASA Space Physics Data Facility. https://doi.org/10.48322/45bb-8792
Pickett, J. S., Chen, L.-J., Kahler, S. W., Santolík, O., Goldstein, M. L., Lavraud, B., et al. (2005). On the generation of solitary waves observed by Cluster in the near-Earth magnetosheath. *Nonlinear Processes in Geophysics*, *12*(2), 181–193. https://doi.org/10.5194/npg-12-181-2005
Pickett, J. S., Menietti, J. D., Gurnett, D. A., Tsurutani, B., Kintner, P. M., Klatt, E., & Balogh, A. (2003). Solitary potential structures observed in the magnetosheath by the Cluster spacecraft. *Nonlinear Processes in Geophysics*, *10*(1/2), 3–11. https://doi.org/10.5194/npg-10-3-2003
Plaschke, F., Hietala, H., & Angelopoulos, V. (2013). Anti-sunward high-speed jets in the subsolar magnetosheath. *Annales Geophysicae*, *31*(10), 1877–1889. https://doi.org/10.5194/angeo-31-1877-2013
Plaschke, F., Hietala, H., Archer, M., Blanco-Cano, X., Kajdič, P., Karlsson, T., et al. (2018). Jets downstream of collisionless shocks. *Space Science Reviews*, *214*(5), 81. https://doi.org/10.1007/s11214-018-0516-3

Plaschke, F., Hietala, H., & Vörös, Z. (2020). Scale sizes of magnetosheath jets. *Journal of Geophysical Research: Space Physics*, *125*(9), e27962. https://doi.org/10.1029/2020JA027962

PlasmaPy Community, Everson, E., Stańczak, D., Murphy, N. A., Kozlowski, P. M., Malhotra, R., et al. (2021). *Plasmapy*. Zenodo. https://doi.org/10.5281/zenodo.5247589

Pokhotelov, O., Sagdeev, R., Balikhin, M., & Treumann, R. (2004). Mirror instability at finite ion-larmor radius wavelengths. *Journal of Geophysical Research*, *109*(A9), A09213. https://doi.org/10.1029/2004ja010568

Pollock, C., Moore, T., Jacques, A., Burch, J., Gliese, U., Saito, Y., et al. (2016). Fast plasma investigation for magnetospheric multiscale. *Space Science Reviews*, *199*(1), 331–406. https://doi.org/10.1007/s11214-016-0245-4

Pritchett, P., Mozer, F., & Wilber, M. (2012). Intense perpendicular electric fields associated with three-dimensional magnetic reconnection at the subsolar magnetopause. *Journal of Geophysical Research*, *117*(A6), A06212. https://doi.org/10.1029/2012ja017533

Raptis, S., Aminalragia-Giamini, S., Karlsson, T., & Lindberg, M. (2020). Classification of magnetosheath jets using neural networks and high resolution OMNI (HRO) data. *Frontiers in Astronomy and Space Sciences*, *7*, 24. https://doi.org/10.3389/fspas.2020.00024

Raptis, S., Karlsson, T., Vaivads, A., Lindberg, M., Johlander, A., & Trollvik, H. (2022). On magnetosheath jet kinetic structure and plasma properties. *Geophysical Research Letters*, *49*(21), e2022GL100678. https://doi.org/10.1029/2022gl100678

Robert, P., Roux, A., Harvey, C. C., Dunlop, M. W., Daly, P. W., & Glassmeier, K.-H. (1998). Tetrahedron geometric factors. *Analysis methods for multi-spacecraft data*, *1*, 323–328.

Rodriguez, P. (1979). Magnetosheath electrostatic turbulence. *Journal of Geophysical Research*, *84*(A3), 917–930. https://doi.org/10.1029/ja084ia03p00917

Russell, C., Anderson, B., Baumjohann, W., Bromund, K., Dearborn, D., Fischer, D., et al. (2016). The magnetospheric multiscale magnetometers. *Space Science Reviews*, *199*(1), 189–256. https://doi.org/10.1007/s11214-014-0057-3

Sahraoui, F., Pinçon, J. L., Belmont, G., Rezeau, L., Cornilleau-Wehrlin, N., Robert, P., & Chanteur, G. (2003). ULF wave identification in the magnetosheath: The k-filtering technique applied to cluster II data. *Journal of Geophysical Research*, *108*(A9), 1335. https://doi.org/10.1029/2002JA009587

Santolík, O., Parrot, M., & Lefeuvre, F. (2003). Singular value decomposition methods for wave propagation analysis. *Radio Science*, *38*(1), 10–11. https://doi.org/10.1029/2000rs002523

Shin, K., Kojima, H., Matsumoto, H., & Mukai, T. (2005). Electrostatic quasi-monochromatic waves downstream of the bow shock: Geotail observations. In *COSPAR colloquia series* (Vol. 16, pp. 293–296). Elsevier. https://doi.org/10.1016/S0964-2749(05)80044-7

Shin, K., Kojima, H., Matsumoto, H., & Mukai, T. (2007). Electrostatic quasi-monochromatic waves in the downstream region of the Earth's bow shock based on geotail observations. *Earth Planets and Space*, *59*(2), 107–112. https://doi.org/10.1186/BF03352683

Smith, E. J., Holzer, R. E., & Russell, C. T. (1969). Magnetic emissions in the magnetosheath at frequencies near 100 Hz. *Journal of Geophysical Research*, *74*(11), 3027–3036. https://doi.org/10.1029/JA074i011p03027

Smith, E. J., & Tsurutani, B. T. (1976). Magnetosheath lion roars. *Journal of Geophysical Research*, *81*(13), 2261–2266. https://doi.org/10.1029/ja081i013p02261

Southwood, D. J., & Kivelson, M. G. (1993). Mirror instability: 1. Physical mechanism of linear instability. *Journal of Geophysical Research*, *98*(A6), 9181–9187. https://doi.org/10.1029/92ja02837

Steinvall, K., Khotyaintsev, Y. V., & Graham, D. B. (2022). On the applicability of single-spacecraft interferometry methods using electric field probes. *Journal of Geophysical Research: Space Physics*, *127*(3), e2021JA030143. https://doi.org/10.1029/2021ja030143

Stenzel, R. L. (1999). Whistler waves in space and laboratory plasmas. *Journal of Geophysical Research*, *104*(A7), 14379–14395. https://doi.org/10.1029/1998JA900120

Svenningsson, I., Yordanova, E., Cozzani, G., Khotyaintsev, Y., & André, M. (2022). Kinetic generation of whistler waves in the turbulent magnetosheath. *Geophysical Research Letters*, *49*(15), e2022GL099065. https://doi.org/10.1029/2022gl099065

Thorne, R., & Tsurutani, B. (1981). The generation mechanism for magnetosheath lion roars. *Nature*, *293*(5831), 384–386. https://doi.org/10.1038/293384a0

Tsurutani, B. T., Smith, E. J., Anderson, R. R., Ogilvie, K. W., Scudder, J. D., Baker, D. N., & Bame, S. J. (1982). Lion roars and nonoscillatory drift mirror waves in the magnetosheath. *Journal of Geophysical Research*, *87*(A8), 6060–6072. https://doi.org/10.1029/JA087iA08p06060

Yao, S., Shi, Q., Liu, J., Yao, Z., Guo, R., Ahmadi, N., et al. (2018). Electron dynamics in magnetosheath mirror-mode structures. *Journal of Geophysical Research: Space Physics*, *123*(7), 5561–5570. https://doi.org/10.1029/2018ja025607

Zhao, J. S., Wang, T. Y., Dunlop, M. W., Shi, C., He, J. S., Dong, X. C., et al. (2019). Large-amplitude electromagnetic ion cyclotron waves and density fluctuations in the flank of the Earth's magnetosheath. *Geophysical Research Letters*, *46*(9), 4545–4553. https://doi.org/10.1029/2019GL081964